



# Synthesis and characterization of Cr<sub>2</sub>C MXenes

Otitoaleke Akinola<sup>1,a)</sup>, Isha Chakraborty<sup>1</sup>, Hugo Celio<sup>2</sup>, Deji Akinwande<sup>1</sup>, Iean Anne C. Incorvia<sup>1</sup>

Received: 3 March 2021; accepted: 21 May 2021; published online: 14 June 2021

MXenes are a large class of materials that are chemically exfoliated from metal–aluminum–carbon (MAX) bulk crystals into low-dimensional sheets. While many MXenes have been theoretically predicted, the careful balance required in the exfoliation between breaking the inter-layer bonds without damaging the intra-layer bonds of the sheets has limited synthesis and experimental study. Here, we developed the synthesis of  $Cr_2C$  from its parent  $Cr_2AlC$  MAX phase and showed the etching is optimized using sodium fluoride and hydrogen chloride with a modified minimally intensive layer delamination (mMILD) method in a cold environment of 9  $^{\circ}C$ . We further optimized the intercalation and delamination using sonication and washing methods. The resulting  $Cr_2C$  crystal structure was characterized. These results open up  $Cr_2C$  to experimental study, including of its predicted emergent magnetic properties, and develop guidelines for synthesizing new MXene materials.

#### Introduction

MXenes are a large class of two-dimensional (2D) layered transition metal carbides and/or nitrides, discovered in 2011 [1], with the general formula  $M_{n+1}X_nT_m$ . They are derived by the selective removal of the A layers from MAX phases, which are ternary carbides, nitrides, or carbonitrides with the general formula  $M_{n+1}AX_n$  (n=1-3); where M= an early transition metal, e.g. Ti, V, Cr, and Mo; A= a group 13 or 14 element; X=C or N; and  $T_m$  is a surface functional group, e.g. OH, O or F. The MAX phase is structured such that the stacks of  $M_{n+1}X_n$  nanosheets are interleaved with A layers which can be chemically etched out. This results in weakly bonded  $M_{n+1}X_n$  layers which can be exfoliated into MXenes, as illustrated in Fig. 1 using Vesta visualization software.

MXenes have been shown and predicted to have numerous useful mechanical and electronic properties [2, 3], and have found applications in electrode materials [4–6], sensors, catalysis [7], energy storage [5, 6, 8–11], and carbon capture [12]. MXenes can also have magnetic properties [13]. For example, from theory, pristine  $Ti_2C$  and  $Ti_2N$  are nearly half-metallic ferromagnets,  $Cr_2N$  is antiferromagnetic, and  $Cr_2C$  is a half-metallic ferromagnet which can undergo ferromagnetic metallic to anti-ferromagnetic insulating state transitions [13]. However,

work needs to be done to synthesize these MXene species to test and use their predicted properties.

In particular, the Cr<sub>2</sub>C MXene, which has a trigonal crystal structure and P3m1 [164] space group, is produced by selectively etching Al atoms from the MAX phase Cr2AlC with a hexagonal crystal structure and P6<sub>3</sub>/mmc [194] space group [11, 14-17]. Two-dimensional Cr2C MXenes have been predicted, using density functional theory calculations, to have ferromagnetic behavior in which the itinerant Cr d electrons are 100% spin polarized around the Fermi surface, resulting in intrinsic half-metallicity with a gap as large as 2.85 eV [15]. This half-metallicity in Cr<sub>2</sub>C MXenes is completely intrinsic, in contrast to low-dimensional materials such as graphene or transition metal dichalcogenides which need strong external electric field or carefully selective doping to induce half-metallicity [15]. Cr<sub>2</sub>C has also been predicted to demonstrate a ferromagnetic-to-antiferromagnetic transition accompanied by a metal-to-insulator transition when the surface is functionalized with F, OH, H, or Cl groups due to the localization of the Cr d electrons [15]. The energy gap is also tunable by the choice of the functional group [15]. This makes Cr<sub>2</sub>C MXenes potentially attractive for nanoscale spintronics applications if Cr<sub>2</sub>C MXene nanosheets could be reliably produced experimentally.

<sup>&</sup>lt;sup>1</sup>Department of Electrical and Computer Engineering, The University of Texas at Austin, Austin, USA

<sup>&</sup>lt;sup>2</sup> Texas Materials Institute, The University of Texas at Austin, Austin, USA

a) Address all correspondence to this author. e-mail: otitoaleke@utexas.edu



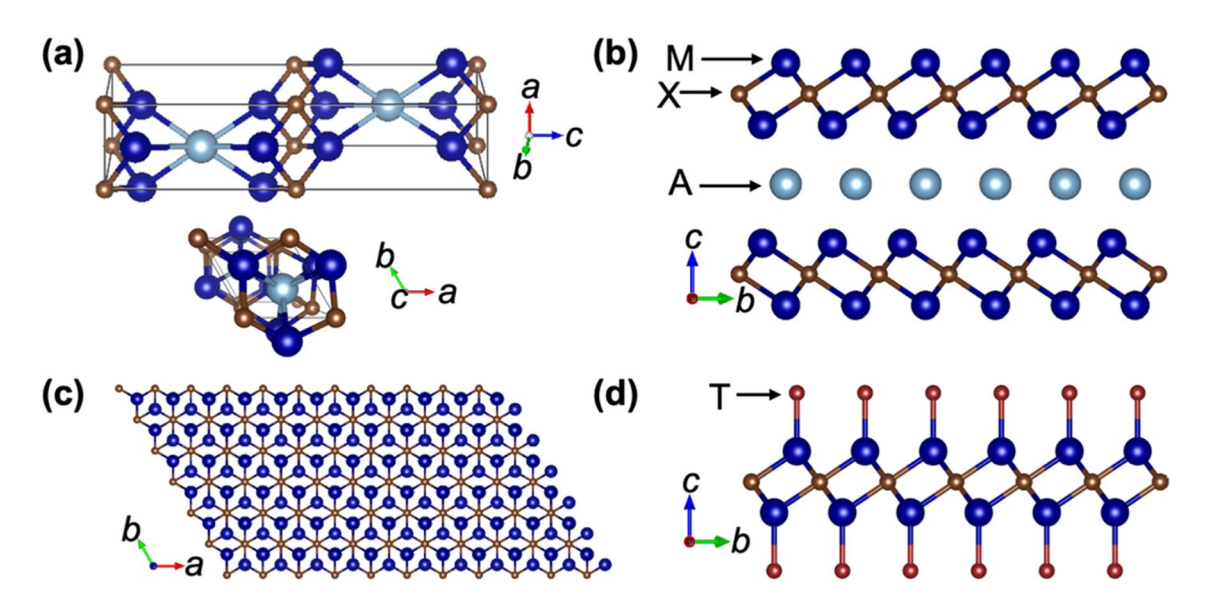


**Figure 1:** MAX and MXene crystal structure. Cartoon images of: (a) The MAX phase; the view along the  $\hat{c}$  direction is shown in the inset. (b) Unetched MAX phase along the  $\hat{a}$  direction, with elements identified as transition metal M (Cr in this case), group III element A (Al in this case), and carbon or nitrogen X (carbon in this case) to form  $Cr_2AlC$ . The A atoms are chemically etched to produced  $Cr_2C$  MXenes, shown in (c) in the  $\hat{c}$  direction after etching. (d)  $Cr_2C$  MXene sheet in the  $\hat{a}$  direction after surface functionalization, where T is an F, O, H or OH radical.

There are three main methods seen in literature for deriving MXenes from the corresponding MAX phase: the use of hydrofluoric (HF) acid, the use of a fluoride salt and an acid, or the use of ammonium bifluoride [2, 18]. In this experiment, fluoride salts and hydrochloric acid were used as the etchant due to the high yield and milder nature of the resulting reaction compared to the use of HF [2, 3, 18]. In addition, it is considered to be a safer method when compared to direct handling of HF [2, 18]. The chemical reaction equation to derive  $Cr_2C$  from  $Cr_2AlC$  is given as follows:

$$\begin{split} 2Cr_2AlC(s) + 6XF(s) + 6HCl(l) &\xrightarrow{yields} 2Cr_2C(s) \\ + 2AlF_3\big(aq\big) + 6XCl + 3H_2\big(g\big) \end{split}$$

where X is a cationic element such as Na or Li; (s), (l), (aq), and (g) imply the materials are in solid, liquid, aqueous, and gaseous states, respectively.

Here, we develop a chemical exfoliation process to reduce the Cr<sub>2</sub>AlC MAX phase into Cr<sub>2</sub>C MXene. To achieve optimal etching results, we varied the fluoride salt used, the reaction environment temperature, the concentration of the reactants, and the after-etch extraction procedure (including speed of centrifugation, method of product separation, and delamination technique), as described subsequently. We discuss how changing these different parameters affect the characteization results, including scanning electron microscopy (SEM) images, electron dispersive x-ray spectroscopy (EDX), X-ray diffraction (XRD), and x-ray photoelectron spectroscopy (XPS) measurements done both on the bulk and exfoliated samples. We also identify the Raman signature and the transmission electron microscopy

(TEM) structure of the synthesized Cr<sub>2</sub>C. The results show that the best exfoliation, i.e. highest yield, lowest byproduct, fastest etch time, and largest area sheets, was acheived using a modified MILD (mMILD) method with sodium fluoride (NaF) salt and hydrochloric acid (HCl) in a 9 °C environment.

## **Results and discussion**

## **Physical morphology**

Figure 2a and b show the physical structure of the unetched  $Cr_2AlC$  under SEM. Using LiF and HCl as etchant at room temperature after 72 h of etch, the  $Cr_2C$  MXene sheets began to become visible as the  $Cr_2AlC$  bulk blocklike structure began to transform into an accordion structure as though a book is drenched in water, taken out, and dried. This structure is shown in Fig. 2c and d. After 96 h the MXene was fully etched, shown in Fig. 2e and f where example stacks of MXene sheets are surrounded by byproducts.

The etch results were further improved, to achieve higher yield, lower byproduct, and shorter etch time, by using the mMILD technique, a cold environment of 9 °C, and using NaF+HCl as the etchant, with results shown in Fig. 3. The mMILD technique used was an adaptation of the MILD method that has proven successful for etching titanium-based MXenes, where the concentration of the fluoride salt and acid is increased and sonication is decreased [2, 10, 18–22]. Here, the concentration of the fluoride salt and acid was kept lower than in the original MILD method, since too high a concentration damaged the MXene sheets.



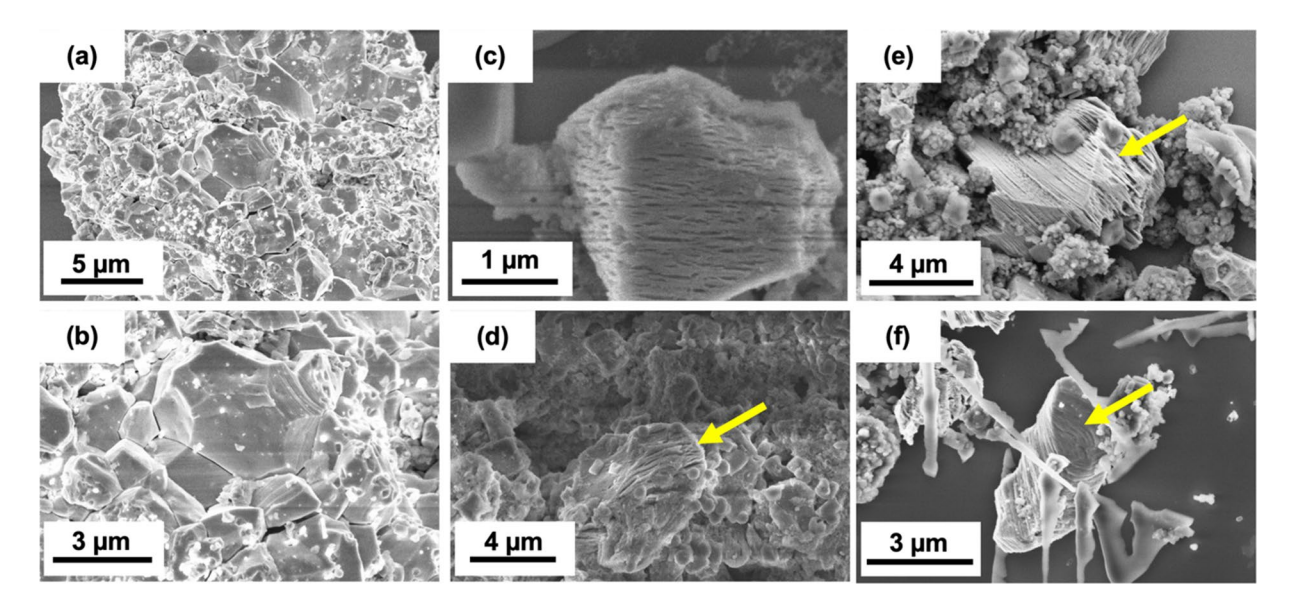


Figure 2: Etch process over time. SEM images of (a), (b) unetched  $Cr_2AlC$  MAX phase. (c), (d)  $Cr_2C$  MXenes after 72 h of etching, and (e), (f)  $Cr_2C$  MXenes after 96 h of etching, all in a mixture of LiF and HCl. The accordion-shaped structure signifies that the inter-MXene Aluminum layer has been etched off by the fluoride salt and hydrochloric acid mixture. (c) shows how the structure looks midway through the etch. Arrows indicate example  $Cr_2C$  sheets.

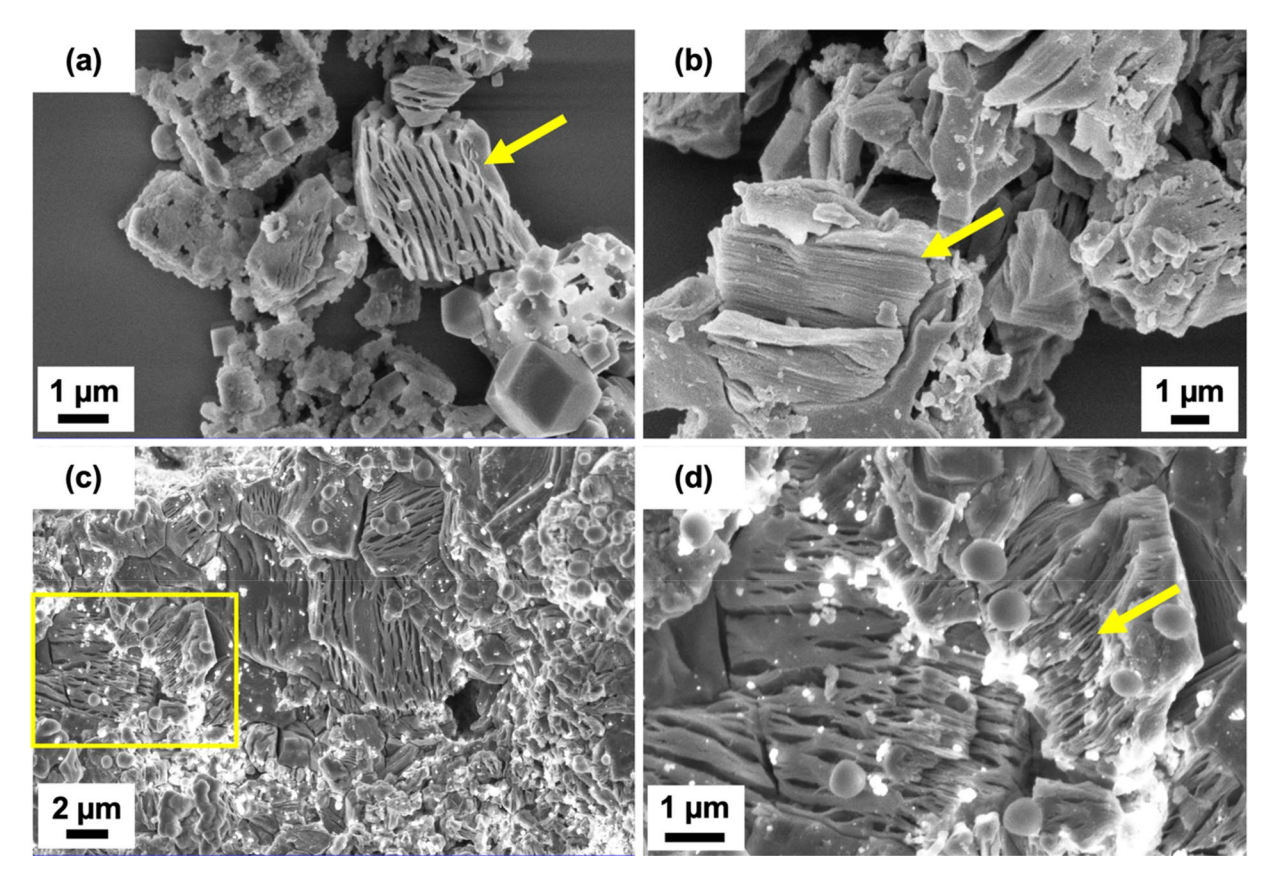


Figure 3: Optimized etch conditions comparing etchants. All images show the etch product after 45 h of etching in 9 °C environment using the mMILD method. (a) Using LiF etchant. (b) Using NaF etchant. (c) Larger area using NaF etchant, with yellow box area shown in (d). Arrows indicate example Cr<sub>2</sub>C sheets.



When the reaction temperature was swept between 9 °C, room temperature, and 50 °C, we found the optimized etch time was 45 h, 96 h, and 120 h, respectively. Since the reaction is exothermic, reducing the temperature will drive the reaction more towards the product side. The benefit of cold temperature is contrary to what has been observed in other works, where better etch results were reported at higher temperatures [23–26], since the increased temperature increases the solubility of the fluoride salts, liberating more of the fluoride ions to take part in the reaction while the cations can take part in the intercalation. Here, since the mMILD method already provided high molar concentrations of the fluoride salts, the higher temperature was not needed, and the low temperature helped to drive the reaction forward.

Figure 3 compares the use of LiF and NaF. In Fig. 3a, LiF is used as the etchant, which produces accordion structures, but with fluorine residue visible as a fuzzy surface on the crystals, confirmed by EDX. We expect less residue using NaF, since NaF solubility is 4.13 g/L compared to LiF solubility of 1.34 g/L [27]. Hence, at the end of the reaction there will be four times less undissolved NaF in the solution. These fluorine atoms and radicals can adhere to the surface of the MXene product.

Figure 3b–d show the results using NaF. Figure 3b shows an example of a clean, low-residue accordion structure achieved with this optimized method, looking like pages of a book. This structure gives proof of successful reduction of the MAX phase Cr<sub>2</sub>AlC to Cr<sub>2</sub>C MXene sheets. Figure 3c shows a larger area with many accordion structures visible, showing the high yield. Figure 3d highlights the yellow box area to show an example structure in more detail. Washing the etch product in HCl before washing in DI water further helped reduce residual salts and byproducts in the etch product mix.

In Fig. 4, the process was further optimized to increase delamination, increase yield, and reduce byproduct. Tetrabutylammonium hydroxide (TBAOH) was used to attempt to further delaminate the sheets [2, 19, 20, 28–30], but as can be seen in Fig. 4a, it introduced more organic impurities into the mix. These organics adhered to the dangling bonds left as the result of the etch, visible as smears of amorphous material on the MXene products. Figure 4b shows the effect of not using TBAOH at all. The cation in the fluoride salt is sufficient for intercalation and delamination of the MXene sheets. Washing to a pH of about 7 ensures that most of the salt has been removed and that the cations are well-intercalated in-between the MXene

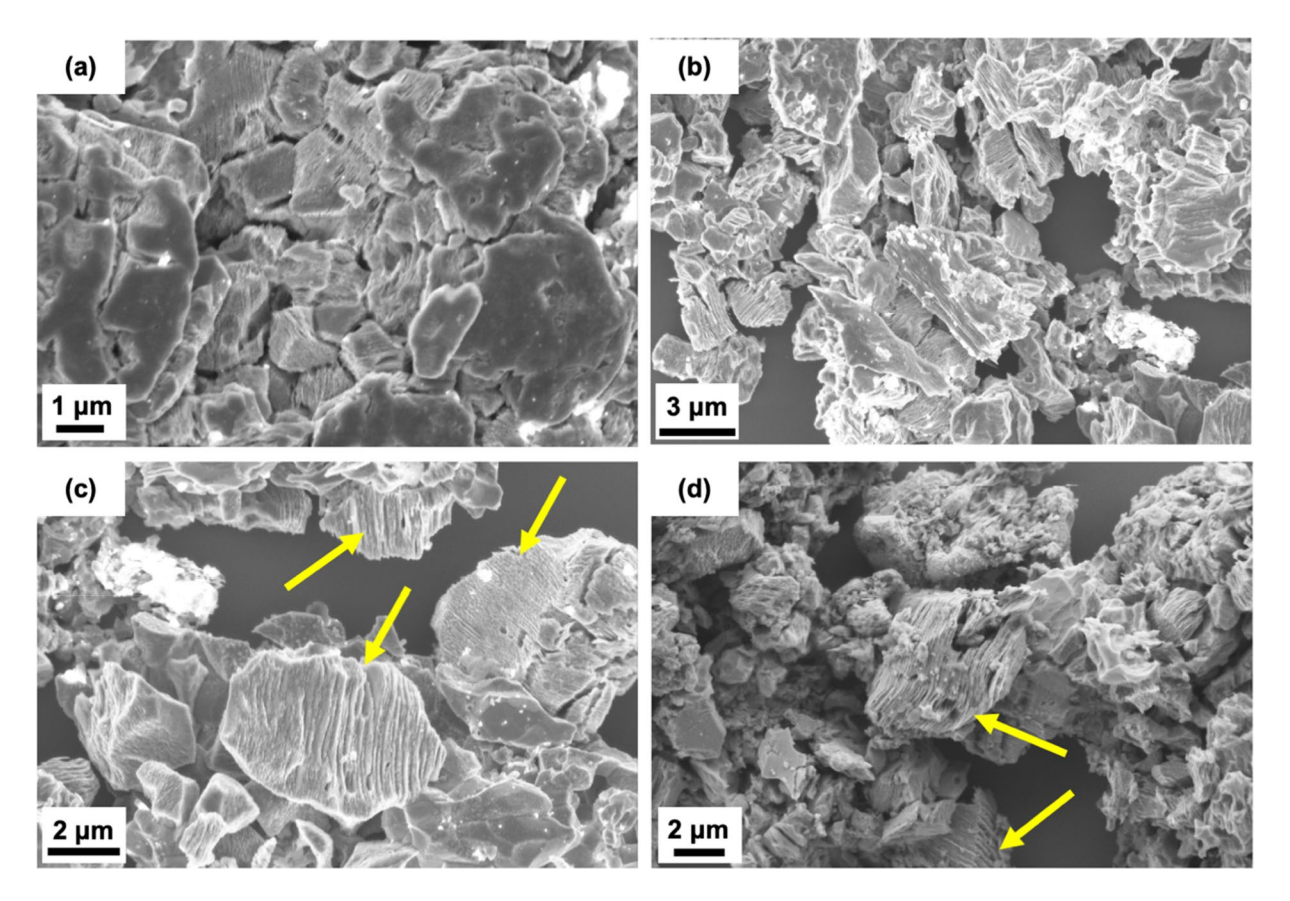


**Figure 4:** Optimized etch conditions using NaF etchant. (a) SEM image of the etch products after using TBAOH, showing increased amorphous material on the surfaces. (b) Etch product without using any TBAOH. (c) Etch product when sonication and HCl wash steps are added, which show improved delamination and yield and reduced byproduct, using the in-lens detector and (d) using secondary electron detector.



sheets. Sonicating the reaction for an hour at the beginning of the etching reaction helps in mixing the reactants and further aids in the intercalation process. It should also be noted that the choice of the centrifuging speed plays a role in preserving the integrity of the MXene sheets. We noticed that using a 2000 rpm rather than a 3500 rpm centrifuging speed helped to produce better quality products.

Figure 4c and d show example SEM images with improved delamination, high yield, and low byproduct wherein sonication was added in the first hour of the etch to promote delamination, and the reaction product was washed in HCl before washing with DI water. Because salts have lower solubility in lower pH conditions, this helped precipitate the excess unreacted fluoride salts and salt byproducts in the solution, leading to lower byproduct for both salts. The images show better sheet-like structures compared to Fig. 4b.

## **Chemical analysis**

Figure 5 shows the initial elemental analysis using EDX for (a–b) unetched  $Cr_2AlC$ , (c–d) LiF-etched  $Cr_2C$  MXene, and (e–f) NaF-etched  $Cr_2C$  MXene. The Al counts are lower for the etched products vis-à-vis the Cr counts, as compared to that of the unetched material, indicating the Al has been significantly removed. There are also more significant fluorine counts for the LiF-etched  $Cr_2C$  MXene in Fig. 5d when compared to the NaF-etched counterpart in Fig. 5f, corroborating the SEM images that show amorphous fluorine on the MXene surface using the LiF etchant. This is an indication that etching with NaF salt gives a cleaner etch result. Since the Cr L $\alpha$  and the O K $\alpha$  energies are very close, a more accurate method is required for the elemental analysis.

XPS was carried out on the dried MXene samples to analyze the elements present before and after etching and to determine the regions and components of the various binding energies identified in the survey profile in Supplementary Fig. S1. Before measurement, the sample was sputtered for 30 s to remove surface impurities.

Figure 6 shows the XPS signal intensity vs. binding energy before and after the optimized etching for the energy regions of (a) Cr, (b) Al, (c) O, and (d) C. The XPS data shows the etch product has reduced Al and that new binding energies are visible for Cr and C, confirming formation of Cr2C. In Fig. 6a, Cr 2p shows up as a doublet Cr 2p1/2 and Cr 2p3/2. After etching, the Cr signal is stronger, indicating some looseness between the layers as a result of stripping off the interlayer Al atoms making more surface Cr atoms available. In Fig. 6b, after etching the intensities for the Al 2s region peaks reduced considerably and shifted. This signifies that the bulk of the Al component of the Cr<sub>2</sub>AlC was removed and some of the remaining Al formed new compounds as shown in the supplementary Fig. S2. In Fig. 6c, after etching the O 1s peaks did not change significantly in intensity but did slightly shift to higher binding energies also signifying the formation of new oxides.

In Fig. 6d, after etching the intensities of the C 1s peaks increased and shifted, showing that new compounds of carbon were formed in the etching process. The C 1s etched data is further analyzed in Fig. 6e. As shown by the orange, light green, and blue traces, a major contributor to the intense C peak is adventitious carbon with the C–C bond, the C–O bond group, and the C=O bond group at binding energies 284.67 eV, 285.85 eV, and 288.02 eV, respectively. These are labeled with C, B, and A, respectively. This is expected because breaking off the Al bonds

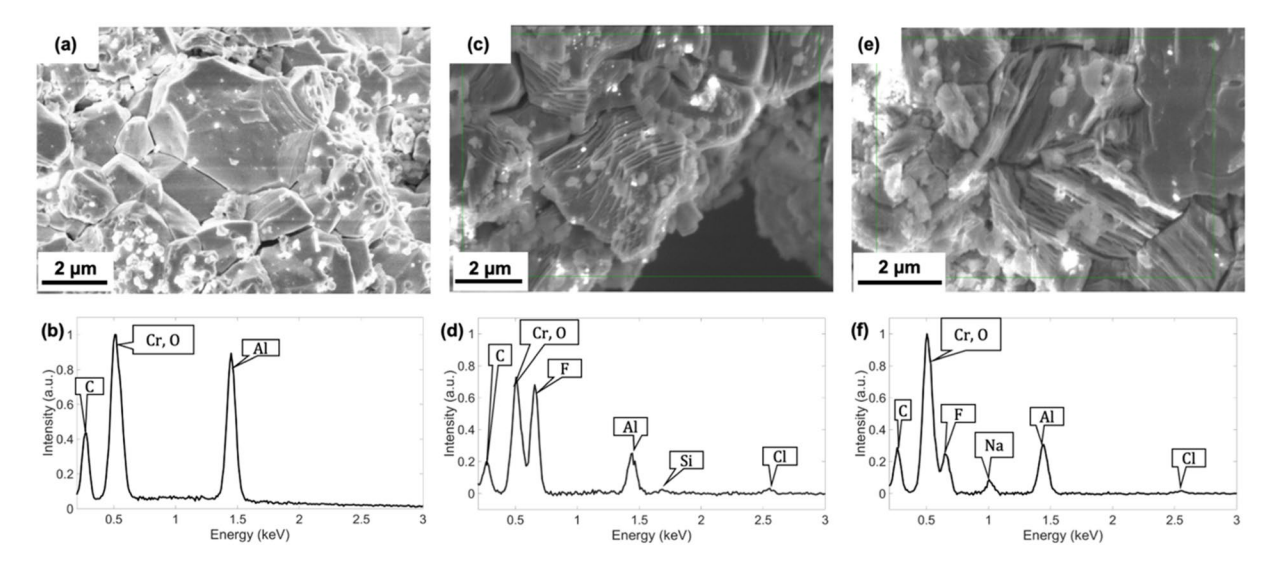


Figure 5: EDX analysis. SEM images of (a) unetched Cr<sub>2</sub>AIC MAX phase, (c) Cr<sub>2</sub>C MXene after etching in LiF and HCl for 45 h, and (e) Cr<sub>2</sub>C MXene after etching in NaF and HCl for 45 h, with corresponding EDX plots in (b), (d), and (f), respectively.



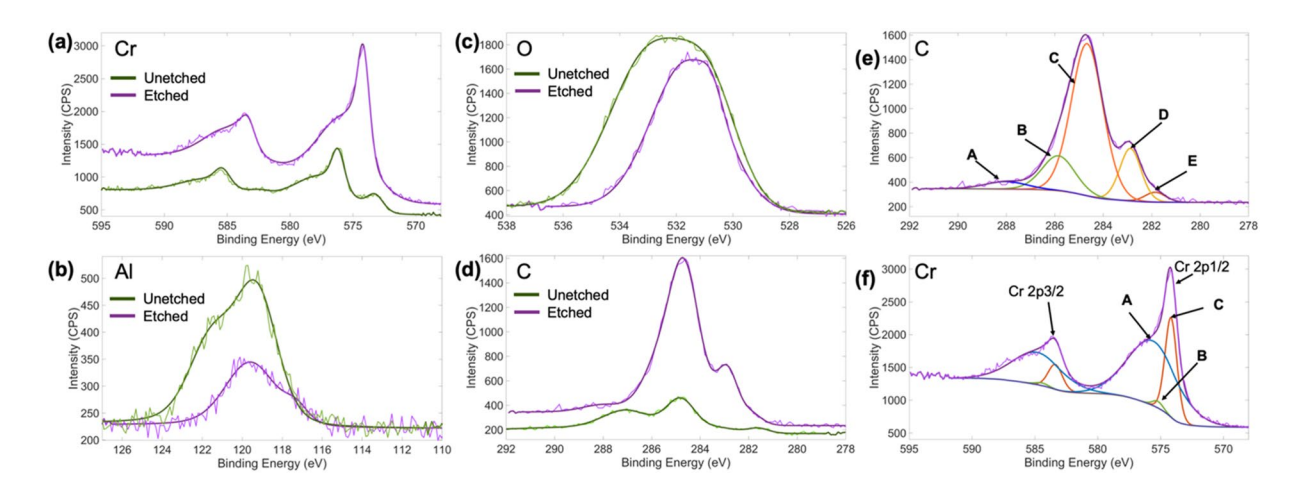


Figure 6: X-ray photoelectron spectroscopy of the unetched  $Cr_2AlC$  MAX phase (green trace) compared to optimized etched  $Cr_2C$  MXene (purple trace). The data are overlayed with an envelope function. (a) Energy region for Cr 3/2p and Cr 1/2p doublets. (b) Energy region for Al 2s. The Al 2p lines are very close to the Cr 3s lines, so the Al 2s lines were observed. (c) Energy region for O 1s. (d) Energy region for C 1s. (e) XPS measurement plots for the C 1s region overlayed with the envelope function (purple trace) and showing different components of  $Cr_7C_3$ ,  $Cr_2C/CrC$ , the C-C adventitious carbon, the C-O bond group, and the C=O bond group, as marked by **E**, **D**, **C**, **B**, **A**, respectively. (f) XPS measurement plots for the Cr 2p region overlayed with the envelope function (purple trace) and showing different components of Cr 2p1/2 and Cr 2p3/2 doublets. The binding energy peaks indicative of  $Cr_7C_3$ ,  $Cr_2C$  and CrC are indicated by **C**, **B**, and **A**, respectively.

in the  $Cr_2AlC$  created more dangling bonds on the Cr for the adventitious C and CO group to latch onto. In addition, the creation of  $Cr_2C$  nanosheets creates more exposed surface area for new surface chemistry. The peak **D** at 282.88 eV is expected to correspond to that of  $Cr_2C$ , while peak **E** at 281.86 eV is characteristic of  $Cr_2C_3$  [31, 32].

The Cr XPS signal from Fig. 6a is further analyzed in Fig. 6f. The binding energy peaks are identified to the nearest 0.2 eV as  $Cr_7C_3$  at 574.18 eV (peak C) and 583.38 eV. The peak B is conjectured to be a mix of  $Cr_2C$  and CrC at 575.23 eV repeating itself at 584.43 eV, while the peak A at 575.63 eV is thought to be CrC also repeating at 584.83 eV [31, 33–40]. It should be noted that that the peak for CrC shows up more intensely similar to our XRD analysis data. Further work needs to be done to separate out the  $Cr_2C$  and CrC etch products. Additional analysis of the XPS regions and components are included in Supplementary Information.

#### Phase analysis

Figure 7 shows powder XRD peaks for unetched and etched samples. Peaks for  $Cr_2C$  are marked by red crosses,  $Cr_2AlC$  by blue diamonds,  $Cr_7C_3$  by gold triangles, and CrC by black circles. The diffraction peaks for the starting  $Cr_2AlC$  MAX phase material are shown by the black trace in Fig. 7a. The peaks indicating  $Cr_2AlC$  are clear and distinct although there are a few  $Cr_7C_3$  phases also showing up as well.

When the etch is done with NaF and HCl using the mMILD method at 9 °C, more  $Cr_2C$  phases at 27.86°, 37.44°, 40.61°, 74.96°, 81.25° and 82.70° appear as shown in Fig. 7b [38, 39,

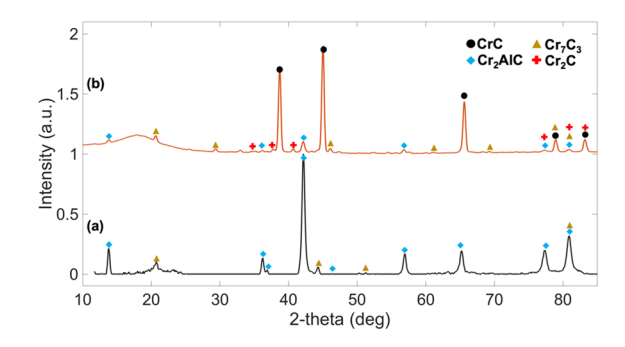


**Figure 7:** Powder X-ray diffraction (XRD) peaks for unetched and etched samples. Peaks for  $Cr_2C$  (red crosses), CrC (black circles),  $Cr_7C_3$  (gold triangles), and  $Cr_2AlC$  (blue diamonds) are marked. (a) Black trace shows the scan of the starting  $Cr_2AlC$  MAX phase material showing distinct peaks for  $Cr_2AlC$  and some trace of  $Cr_7C_3$ . (b) Orange trace shows the result after etched with NaF and HCl at 9 °C for 45 h using the mMILD method. More phases for  $Cr_2C$  are seen [38, 39, 41–44], as well as fewer impurities (unmarked peaks which are mostly impurities from  $Al^{3+}$ ,  $Na^+$ ,  $Cl^-$  or  $F^-$ ) and fewer phases of  $Cr_2AlC$  (blue diamonds) [48] and  $Cr_7C_3$  (gold triangles) [49]. Although intense peaks for CrC also show up [50], lower intensities of  $Cr_2AlC$  indicate that the etch is more successful.

41–44], compared to other methods (see supplementary Information) [41, 45–47]. Since there is limited reliable XRD analysis of Cr<sub>2</sub>C, the peaks identified are conjectured based on what is available. In addition, the intensities for Cr<sub>2</sub>AlC [48] and Cr<sub>7</sub>C<sub>3</sub> [49] reduced compared to the rest of the methods. The complementary appearance of prominent CrC phases [50] in addition to this indicates that after 45 h of etching most of the Al from the starting Cr<sub>2</sub>AlC MAX phase has been etched out. See Supplementary Information for additional XRD analysis of sample degradation over a 2-year period.



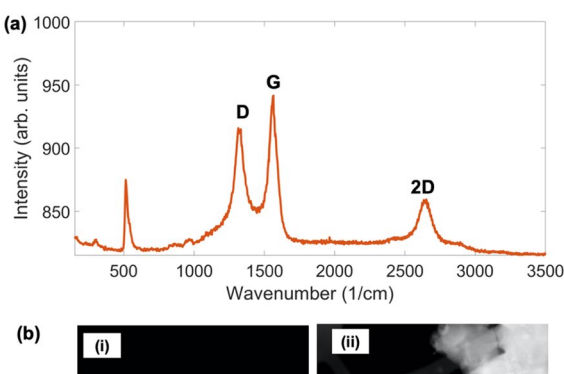
## Additional analysis and discussion

Figure 8a shows the Raman spectra for the etched MXenes. The Raman modes show a D peak at 1327 cm<sup>-1</sup>, a G peak at 1564 cm<sup>-1</sup>, and a 2D peak at 2642 cm<sup>-1</sup>. These peaks in addition to those showing up at 513.7 cm<sup>-1</sup> and 962.2 cm<sup>-1</sup> are believed to be characteristic of chromium carbides [51–53].

The acquired TEM images are shown in Fig. 8b. The structures in (i) and (ii), as identified by the arrow, show striations indicating delaminated MXene sheets. In (iii) and (iv) the boundaries of different layers of the MXene sheets are visible.

#### **Conclusions**

While many MXenes have been theoretically predicted, the careful balance required in the exfoliation between breaking the inter-layer bonds without damaging the intra-layer bonds of the sheets has limited synthesis and experimental study. We have developed a chemical exfoliation process that derives Cr<sub>2</sub>C MXenes from the parent Cr<sub>2</sub>AlC MAX phase. Our results show that the best exfoliation, i.e. highest yield, lowest byproduct, fastest etch time, and largest area sheets, was acheived using our mMILD method with NaF salt and HCl in a 9 °C environment.



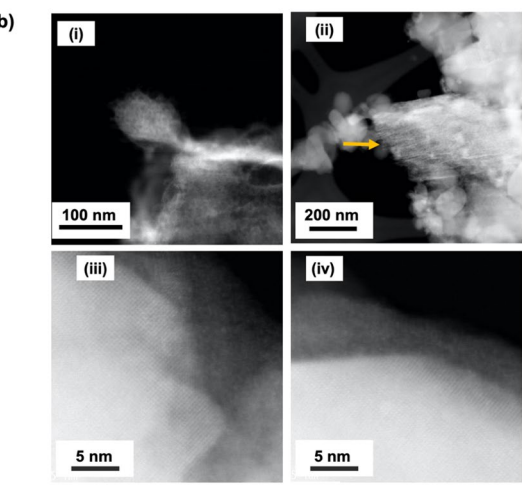


**Figure 8:** (a) Raman spectrum for the etched  $Cr_2C$  MXene. (b) STEM images for the etched  $Cr_2C$  MXene.

In addition, sonicating for the first hour of the reaction and washing in an acid medium before washing in DI water up to a pH of 7 further helped the intercalation and delamination process. Having a proper choice of centrifuging speed helps to preserve the quality of the flakes. A series of analysis including SEM, EDX, XPS and XRD confirm our findings.

The XRD and XPS data shows that a significant amount of CrC is being produced in addition to the intended Cr<sub>2</sub>C MXene, showing further work needs to be done to separate the Cr<sub>2</sub>C from CrC. Overall, these results open up Cr<sub>2</sub>C to experimental study, including of its predicted emergent magnetic properties, and develop guidelines for synthesizing new MXene materials.

# **Experimental methods**

### **Etch procedures**

### Using two fluoride salts

We carried out two separate reactions to compare using Lithium Fluoride (LiF) and Sodium Fluoride (NaF). In two separate beakers, 3 ml of 12 M concentrated Hydrochloric Acid (HCl, J.T. Baker, 37% CMOS grade) was added to 3 ml of DI water to dilute. Then, 0.919 g of LiF (Alfa Aesar, 98.5%) was added to one of the beakers, whereas 1.521 g of NaF (Alfa Aesar, 99%) was added to the other beaker. The two beakers were shaken vigorously for a minute or two to ensure that the fluoride salts dissolve optimally in the acid. Afterwards, 1.728 g of ball-milled Chromium Aluminum Carbide (Cr<sub>2</sub>AlC, ACI Alloys, purity > 99.9%) with average grain size of 1 mm was gradually added to each of the beakers containing the acid-salt solution. On addition of the Cr<sub>2</sub>AlC, the reaction heats up showing exothermicity, there is a release of Hydrogen gas molecules, and the mixture turns dark green as expected.

The reaction sat at room temperature and samples were collected from the reaction after 48 h, 72 h, and 96 h. These samples were washed through five cycles using distilled water and centrifuged at a speed of 3500 rpm for 10 min per cycle. After each cycle, the solute mix was decanted off and fresh distilled water was added for the next cycle.

## Varying the temperature of the reaction environment

To determine the effect of reaction temperature, we put two beakers, one containing  $HCl + NaF + Cr_2AlC$  and the other containing  $HCl + LiF + Cr_2AlC$ , in a heating bath at 50 °C. Another two beakers each with NaF or LiF were put in a cold environment at 9 °C. The reaction sat for 96 h and sampled every 24 h. Cleaning procedures were carried out as described above.



#### Varying reactant concentration using the mMILD method

To observe the effect of varying the reactant concentration, we used a modified minimally intensive layer delamination (mMILD) method [19]. This involved slightly increasing the concentration of the acid and the fluoride salt to release more cations for intercalation and delamination. In two separate beakers, 3 ml of DI water was added to 3 ml of HCl to dilute. Then, 0.783 g of LiF was added to one of the beakers while 1.268 g of NaF was added to the other beaker. The two beakers were shaken vigorously for a minute or two to dissolve the fluoride salts in the acid. Afterwards, 0.576 g of Cr<sub>2</sub>AlC was gradually added to each of the beakers containing the acid-salt solution.

# Achieving better separation and delamination after etching reaction

For better etch quality, the reaction products were first washed in up to 50 ml of HCl before going on to wash with DI water. Washing the etch product in HCl helps to precipitate the remaining fluoride salts and other salt byproducts while the MXene product remains dispersed in acid. The MXene-acid colloid was then decanted into a separate beaker diluted in water and centrifuged to extract the MXene which had settled to the bottom of the centrifuge tube. Afterwards, the supernatant was decanted and the MXene mass was washed several times in DI water until a pH of about 7. In addition, the samples were centrifuged at 2000 rpm for 15 min rather than 3500 rpm for 10 min that was earlier used

We also tested the effect of delamination with Tetrabutylammonium hydroxide (TBAOH). After washing the etch reaction in DI water until a satisfactory pH is achieved, 12.5 ml of TBAOH was added to 1 g of the etched MXene and made to mix on a rotator for 4 h. After, the products are washed in DI water until a pH of about 7.

#### Sample characterization

After the supernatant from the reaction had reached pH of between 6 and 7, the samples were drop-casted on a 1 cm $^2$  silicon chip and dried on a hotplate at about 500 °C. The physical structure of the samples was observed using scanning electron microscopy (SEM, Zeiss Neon 40) with 5 kV beam voltage and the in-lens secondary electron detector.

Initial elemental analysis was carried out using the Bruker electron dispersive X-ray spectrometer (EDX) attached to the SEM. For further elemental analysis, some of the dried

MXene samples were put on a graphite tape and Kratos X-ray Photoelectron Spectrometer was used to analyze the elements present in the sample. After sputtering the surface for 30 s to remove surface impurities, surveys and region scans were made for Cr, O, Al, and C using a step size of 0.05 eV for 580 steps with a dwell time of 1.5 s and a characteristic energy of 1486.6 eV. Further data analysis was carried out with Casa XPS software to identify the regions and components for the various binding energies.

Powder X-ray diffraction (XRD) analysis was carried out on dried samples using a Scintag X1 Theta-Theta Diffractometer and a Rigaku R-Axis Spider Diffractometer, both with monochromatic Cu K $\alpha$  X-ray sources (wavelength 1.54 Å).

Raman analysis was performed on the optimized-etched Cr<sub>2</sub>C MXene using a Witec Micro-Raman Spectrometer Alpha 300 with an Ar laser (wavelength 514 nm). Scanning transmission electron microscopy (STEM) was performed for a closer look into the structure of the etched MXene product, using a IEOL NEOARM.

# **Acknowledgments**

This research was primarily supported by the National Science Foundation through the Center for Dynamics and Control of Materials: an NSF MRSEC under Cooperative Agreement No. DMR-1720595. This work was performed in part at the University of Texas Microelectronics Research Center, a member of the National Nanotechnology Coordinated Infrastructure (NNCI), which is supported by the National Science Foundation (Grant ECCS-2025227). The authors acknowledge the use of shared research facilities supported in part by the Texas Materials Institute, the Center for Dynamics and Control of Materials: an NSF MRSEC (DMR-1720595), and the Texas Nanofabrication Facility supported by NSF Grant No. NNCI-1542159.

## **Data availability**

The datasets generated during and/or analyzed during the current study are available from the corresponding author on reasonable request.

#### **Declarations**

**Conflict of interest** The authors have no conflicts of interest to declare that are relevant to the content of this article.

# **Supplementary Information**

The online version contains supplementary material available at https://doi.org/10.1557/s43578-021-00258-7.



#### References

- M. Naguib, M. Kurtoglu, V. Presser, J. Lu, J. Niu, M. Heon, L. Hultman, Y. Gogotsi, M.W. Barsoum, Two-dimensional nanocrystals produced by exfoliation of Ti<sub>3</sub>AlC<sub>2</sub>. Adv. Mater. 23, 4248–4253 (2011)
- B. Anasori, M.R. Lukatskaya, Y. Gogotsi, 2D metal carbides and nitrides (MXenes) for energy storage. Nat. Rev. Mater. (2017). https://doi.org/10.1038/natrevmats.2016.98
- M. Ghidiu, M.R. Lukatskaya, M.Q. Zhao, Y. Gogotsi, M.W. Barsoum, Conductive two-dimensional titanium carbide 'clay' with high volumetric capacitance. Nature 516, 78–81 (2015)
- Y. Dall'Agnese, P.L. Taberna, Y. Gogotsi, P. Simon, Twodimensional vanadium carbide (MXene) as positive electrode for sodium-ion capacitors. J. Phys. Chem. Lett. 6, 2305–2309 (2015)
- J. Luo, C. Wang, H. Wang, X. Hu, E. Matios, X. Lu, Pillared MXene with ultralarge interlayer spacing as a stable matrix for high performance sodium metal anodes. Adv. Funct. Mater. 1805946, 1–12 (2019)
- J. Luo, X. Lu, E. Matios, C. Wang, H. Wang, Y. Zhang, X. Hu, Tunable MXene-derived 1D/2D hybrid nanoarchitectures as a stable matrix for dendrite-free and ultrahigh capacity sodium metal anode. Nano Lett. (2020). https://doi.org/10.1021/acs. nanolett.0c03215
- Y.W. Cheng, J.H. Dai, Y.M. Zhang, Y. Song, Transition metal modification and carbon vacancy promoted Cr<sub>2</sub>CO<sub>2</sub> (MXenes): a new opportunity for a highly active catalyst for the hydrogen evolution reaction. J. Mater. Chem. A 6, 20956–20965 (2018)
- X. Zou, G. Li, Q. Wang, D. Tang, B. Wu, X. Wang, Energy storage properties of selectively functionalized Cr-group MXenes. Comput. Mater. Sci. 150, 236–243 (2018)
- A. Yadav, A. Dashora, N. Patel, A. Miotello, M. Press, D.C. Kothari, Study of 2D MXene Cr2C material for hydrogen storage using density functional theory. Appl. Surf. Sci. 389, 88–95 (2016)
- S. Sun, C. Liao, A.M. Hafez, H. Zhu, S. Wu, Two-dimensional MXenes for energy storage. Chem. Eng. J. 338, 27–45 (2018)
- D. Sun, Q. Hu, J. Chen, X. Zhang, L. Wang, Q. Wu, A. Zhou, Structural Transformation of MXene (V2C, Cr2C, and Ta2C) with O groups during lithiation: a first-principles investigation. ACS Appl. Mater. Interfaces 8, 74–81 (2016)
- Á. Morales-García, A. Fernández-Fernández, F. Viñes, F. Illas, CO2 abatement using two-dimensional MXene carbides. J. Mater. Chem. A 6, 3381–3385 (2018)
- B. Anasori, Y. Xie, M. Beidaghi, J. Lu, B.C. Hosler, L. Hultman, P.R.C. Kent, Y. Gogotsi, M.W. Barsoum, Two-dimensional, ordered, double transition metals carbides (MXenes). ACS Nano 9, 9507–9516 (2015)
- A. Jain, S.P. Ong, G. Hautier, W. Chen, W.D. Richards, S. Dacek, S. Cholia, D. Gunter, D. Skinner, G. Ceder, K.A.

- Persson, The materials project: a materials genome approach to accelerating materials innovation. APL Mater. 1, 011002 (2013)
- 15. C. Si, J. Zhou, Z. Sun, Half-metallic ferromagnetism and surface functionalization-induced metal-insulator transition in graphene-like two-dimensional  $\rm Cr_2C$  Crystals. ACS Appl. Mater. Interfaces 7, 17510–17515 (2015)
- M. Khazaei, A. Ranjbar, K. Esfarjani, D. Bogdanovski, R. Dronskowski, S. Yunoki, Insights into exfoliation possibility of MAX phases to MXenes. Phys. Chem. Chem. Phys. 20, 8579–8592 (2018)
- M. Khazaei, M. Arai, T. Sasaki, C.-Y. Chung, N.S. Venkataramanan, M. Estili, Y. Sakka, Y. Kawazoe, Novel electronic and magnetic properties of two-dimensional transition metal carbides and nitrides. Adv. Funct. Mater. 23, 2185–2192 (2013)
- B.M. Jun, S. Kim, J. Heo, C.M. Park, N. Her, M. Jang, Y. Huang, J. Han, Y. Yoon, Review of MXenes as new nanomaterials for energy storage/delivery and selected environmental applications. Nano Res. 12, 471–487 (2019)
- 19. X. Sang, Y. Xie, M.W. Lin, M. Alhabeb, K.L. Van Aken, Y. Gogotsi, P.R.C. Kent, K. Xiao, R.R. Unocic, Atomic defects in monolayer titanium carbide  $(\mathrm{Ti}_3\mathrm{C}_2\mathrm{T}_\mathrm{x})$  MXene. ACS Nano 10, 9193–9200 (2016)
- M. Alhabeb, K. Maleski, B. Anasori, P. Lelyukh, L. Clark, S. Sin, Y. Gogotsi, Guidelines for synthesis and processing of twodimensional titanium carbide (Ti<sub>3</sub>C<sub>2</sub>T<sub>x</sub> MXene). Chem. Mater. 29, 7633–7644 (2017)
- J.C. Lei, X. Zhang, Z. Zhou, Recent advances in MXene: preparation, properties, and applications. Front. Phys. 10, 276–286 (2015)
- 22. X.H. Wang, Y.C. Zhou, Layered machinable and electrically conductive  ${\rm Ti_2AlC}$  and  ${\rm Ti_3AlC_2}$  ceramics: a review. J. Mater. Sci. Technol. **26**, 385–416 (2010)
- 23. M. Wu, B. Wang, Q. Hu, L. Wang, A. Zhou, The synthesis process and thermal stability of V2C MXene. Materials (Basel) 11, 8–11 (2018)
- 24. K. Rajavel, T. Ke, K. Yang, D. Lin, Condition optimization for exfoliation of two dimensional titanium carbide  $(Ti_3C_2T_x)$ . Nanotechnology **29**, 095605 (2018)
- L. Li, G. Li, L. Tan, Y. Zhang, B. Wu, Highly efficiently delaminated single-layered MXene nanosheets with large lateral size.
   Langmuir 33, 9000–9006 (2017)
- A. Feng, Y. Yu, Y. Wang, F. Jiang, Y. Yu, L. Mi, L. Song, Twodimensional MXene Ti3C2 produced by exfoliation of Ti3AlC2. Mater. Des. 114, 161–166 (2017)
- 27. W.M. Haynes, D.R. Lide, T.J. Bruno, CRC Handbook of Chemistry and Physics: A Ready-Reference Book of Chemical and Physical Data (CRC Press, Boca Raton, 2016).
- 28. K. Huang, Z. Li, J. Lin, G. Han, P. Huang, Two-dimensional transition metal carbides and nitrides (MXenes) for biomedical applications. Chem. Soc. Rev. 47, 5109–5124 (2018)



- J. Halim, S. Kota, M.R. Lukatskaya, M. Naguib, M.Q. Zhao, E.J. Moon, J. Pitock, J. Nanda, S.J. May, Y. Gogotsi, M.W. Barsoum, Synthesis and characterization of 2D Molybdenum Carbide (MXene). Adv. Funct. Mater. 26, 3118–3127 (2016)
- 30. P. Urbankowski, B. Anasori, T. Makaryan, D. Er, S. Kota, P.L. Walsh, M. Zhao, V.B. Shenoy, M.W. Barsoum, Y. Gogotsi, Synthesis of two-dimensional titanium nitride  ${\rm Ti_4N_3}$  (MXene). Nanoscale **8**, 11385–11391 (2016)
- NIST X-ray Photoelectron Spectroscopy Database. NIST Standard Reference Database Number 20 (2000). https://doi.org/10. 18434/T4T88K
- Thermo Scientific. XPS Interpretation of Carbon. (2016). http:// xpssimplified.com/elements/carbon.php. Accessed 25 Feb 2021
- E.I. Zamulaeva, E.A. Levashov, E.A. Skryleva, T.A. Sviridova,
   P.V. Kiryukhantsev-Korneev, Conditions for formation of MAX
   phase Cr2AlC in electrospark coatings deposited onto titanium
   alloy. Surf. Coat. Technol. 298, 15–23 (2016)
- 34. D.B. Lee, T.D. Nguyen, S.W. Park, Corrosion of  $Cr_2AlC$  in  $Ar/1\%SO_2$  gas between 900 and 1200  $^{\circ}C$ . Oxid. Met. **75**, 313–323 (2011)
- A. Obrosov, R. Gulyaev, A. Zak, M. Ratzke, M. Naveed, W. Dudzinski, S. Weiß, Chemical and morphological characterization of magnetron sputtered at different bias voltages Cr-Al-C coatings. Materials (Basel) 10, 1–16 (2017)
- I. Grohmann, E. Kemnitz, A. Lippitz, W.E.S. Unger, Curve fitting of Cr 2p photoelectron spectra of Cr<sub>2</sub>O<sub>3</sub> and CrF<sub>3</sub>. Surf. Interface Anal. 23, 887–891 (1995)
- Z.M. Khamdokhov, Z.K. Kalazhokov, R.S. Teshev, K.H.
   Kalazhokov, Chromium-nickel alloy for the synthesis of carbon nanoparticles. Nano Hybrids Compos. 28, 123–129 (2020)
- S. Ma, J. Ye, A. Liu, Y. Liu, J. Wang, J. Pang, I. Reimanis, Synthesis, characterization, and consolidation of Cr2(C, N) solid solution powders. J. Am. Ceram. Soc. 99, 1943–1950 (2016)
- S.M. Schmuecker, D. Clouser, T.J. Kraus, B.M. Leonard, Synthesis
  of metastable chromium carbide nanomaterials and their electrocatalytic activity for the hydrogen evolution reaction. Dalt. Trans.
  46, 13524–13530 (2017)
- 40. Electronic Supplementary Material (ESI) for Dalton Transactions . This journal is © The Royal Society of Chemistry 2017 Synthesis of Metastable Chromium Carbide Nanomaterials and their Electrocatalytic Activity for the Hydrogen Evolution Reaction Samant (2017).
- 41. F.Z. Abderrahim, H.I. Faraoun, T. Ouahrani, Structure, bonding and stability of semi-carbides M 2C and sub-carbides M 4C

- (M=V, Cr, Nb, Mo, Ta, W): a first principles investigation. Phys. B Condens. Matter **407**, 3833–3838 (2012)
- 42. H. Lux, L. Eberle, Zur Kenntnis der Chrom(II)-Salze und des Chrom(II)-oxids III. Chem. Ber. **94**, 1562–1571 (1961)
- Q.T.H. Ta, N.M. Tran, J.S. Noh, Pressureless manufacturing of Cr<sub>2</sub>AlC compound and the temperature effect. Mater. Manuf. Process. 36, 200–208 (2021)
- S. Loubière, C. Laurent, J.P. Bonino, A. Rousset, Powders of chromium and chromium carbides of different morphology and narrow size distribution. Mater. Res. Bull. 33, 935–944 (1998)
- 45. E. Bouzy, E. Bauer-Grosse, G. Le Caër, Naci and filled re3b-type structures for two metastable chromium carbides. Philos. Mag. B **68**, 619–638 (1993)
- W. Jeitschko, H. Nowotny, F. Benesovsky, Carbon-containing ternary compounds (H-Phase). Monatsh. Chem. 94, 672–676 (1963)
- 47. M.A. Rouault, P. Herpin, M.R. Fruchart, Crystallographic study of carbides Cr7C3 and Mn7C2. *Ann. Chim. Fr.* (1970)
- M. Li, J. Wang, Z. Lin, Y. Zhou, In-situ hot pressing/solid-liquid reaction synthesis of bulk Cr2AlC. researchgate.net (2005). https://doi.org/10.3139/146.101033
- H.F. McMurdie, M.C. Morris, E.H. Evans, B. Paretzkin, W. Wong-Ng, L. Ettlinger, C.R. Hubbard, Standard X-ray diffraction powder patterns from the JCPDS Research Associateship. Powder Diffr. 1, 64–77 (1986)
- E. Bouzy, E. Bauer-Grosse, G. Le Caër, NaCl and filled Re3B-type structures for two metastable chromium carbides. Philos. Mag. B 68, 619–638 (1993)
- T. Thomberg, H. Kurig, A. Jänes, E. Lust, Mesoporous carbidederived carbons prepared from different chromium carbides. Microporous Mesoporous Mater. 141, 88–93 (2011)
- C. Avril, V. Malavergne, R. Caracas, B. Zanda, B. Reynard, E. Charon, E. Bobocioiu, F. Brunet, S. Borensztajn, S. Pont, M. Tarrida, F. Guyot, Raman spectroscopic properties and Raman identification of CaS-MgS-MnS-FeS-Cr2FeS4 sulfides in meteorites and reduced sulfur-rich systems. Meteorit. Planet. Sci. 48, 1415–1426 (2013)
- K. Nygren, M. Samuelsson, A. Flink, H. Ljungcrantz, Å. Kassman Rudolphi, U. Jansson, Growth and characterization of chromium carbide films deposited by high rate reactive magnetron sputtering for electrical contact applications. Surf. Coat. Technol. 260, 326–334 (2014)